SPECTRAL ENERGY DISTRIBUTIONS OF PASSIVE T TAURI DISKS: INCLINATION

E. I. CHIANG AND P. GOLDREICH
California Institute of Technology, Pasadena, CA 91125; echiang@tapir.caltech.edu, pmg@nicholas.caltech.edu

ABSTRACT

We compute spectral energy distributions (SEDs) for passive T Tauri disks viewed at arbitrary inclinations. Semianalytic models of disks in radiative and hydrostatic equilibrium are employed. Over viewing angles for which the flared disk does not occult the central star, the SED varies negligibly with inclination. For such aspects, the SED shortward of ~ 80 μm is particularly insensitive to orientation, since short wavelength disk emission is dominated by superheated surface layers, which are optically thin. The SED of a nearly edge-on disk is that of a class I source. The outer disk occults inner disk regions, and emission shortward of ~ 30 μm is dramatically extinguished. Spectral features from dust grains may appear in absorption. However, millimeter-wavelength fluxes decrease by at most a factor of 2 from face-on to edge-on orientations. We present illustrative applications of our SED models. The class I source 04108+2803B is considered a T Tauri star hidden from view by an inclined circumstellar disk. Fits to its observed SED yield model-dependent values for the disk mass of ~ 0.015 $M_\odot$ and a disk inclination of $\sim 65°$ relative to face-on. The class II source GM Aur represents a T Tauri star only slightly obscured by its circumstellar disk. Fitted parameters include a disk mass of ~ 0.050 $M_\odot$ and an inclination of $\sim 60°$, where the viewing angle is chosen to reproduce the observed visual extinction of $A_V = 0.5$ mag.

Subject headings: accretion, accretion disks — circumstellar matter — radiative transfer — stars: individual (GM Aurigae, 04108+2803B) — stars: pre–main-sequence

1. INTRODUCTION

Excess infrared (IR) emission from T Tauri stars is thought to originate from circumstellar disks (Mendoza 1968; Shu, Adams, & Lizano 1987, and references therein). Passive disks are the simplest to consider. By definition, they lack intrinsic luminosity and reradiate the energy they absorb from the central star.

Hydrostatic, radiative equilibrium models for passive T Tauri disks are derived by Chiang & Goldreich (1997, hereafter CG97). The disk surface flares outward with increasing radius and intercepts more stellar radiation, especially at large distances from the central star, than a flat disk would (Kenyon & Hartmann 1987). An optically thin layer of superheated dust grains ensheaths the entire disk. Dust grains in this surface layer are directly exposed to central starlight and reradiate to space about half the stellar energy they absorb. The other half is emitted toward the midplane and regulates the temperature of the cooler disk interior. Vertical temperature gradients in externally illuminated disk atmospheres are calculated in detail by Calvet et al. (1991), Malbet & Bertout (1991), and D'Alessio et al. (1998).

CG97 compute spectral energy distributions (SEDs) of passive disks viewed face-on. The calculated SED is fairly constant over the thermal IR, in accord with the observed flattish excesses of T Tauri stars such as GM Aur. Spectral features from dust grains in the superheated layer appear in emission when the disk is viewed face-on, similar to solid-state emission lines evinced by T Tauri stars and Herbig Ae/Be stars (Cohen & Witteborn 1985; Waelkens et al. 1996; Waters & Waelkens 1998).

What is the spectrum of a passive disk whose midplane is inclined at an arbitrary angle, θ, to the plane of the sky? In § 2, model assumptions and results pertaining to the continuum SED are set forth. In § 3, we study how spectral signatures of some dust grain resonances change from emission to absorption as the disk is viewed increasingly edge-on.

Applications to observations are contained in § 4. There, we assess the possibility that the relatively low 12 μm flux of GM Aur might be caused by a nonzero disk inclination, as opposed to a central AU-sized gap. We close by considering whether differences between class I and class II SEDs might reflect differences in viewing angle rather than evolutionary status.[1]

2. INCLINATION DEPENDENCE OF CONTINUUM SED

2.1. Model Assumptions

We consider a passive disk in radiative and hydrostatic balance around a T Tauri star. The model employed is identical to that derived in §§ 2.1 and 2.3 of CG97. Symbols and values of free parameters are listed here in Table 1, and henceforth are used without explanation. We measure position by cylindrical radius, a, and vertical distance above the disk midplane, z.[2]

Derived disk properties relevant to our present investigation are summarized as follows. At each radius we distinguish two regions: the superthermal surface layer, which is directly exposed to light from the central star, and the cooler, diffusively heated interior, which the surface encases. Variables evaluated in the former region are denoted by a subscript s, while those in the latter region carry a subscript i. Pertinent results from CG97 include the dust temperature at the surface

$$T_{ds} \approx \frac{550}{a_{AU}^{2/5}} \text{ K} ,\qquad(1)$$

---

[1] In the classification scheme of Lada & Wilking (1984; see also Lada 1987), class I sources exhibit SEDs that rise from 2 to 10 μm, i.e., $-3 \lesssim n \lesssim 0$, where $\nu F_\nu \propto \nu^n$. For class II sources, $0 \lesssim n \lesssim 2$.
[2] The disk radius in astronomical units is denoted by a_{AU}.

TABLE 1
FREE PARAMETERS

Symbol	Meaning	Value
M_*	Stellar mass	$0.5\ M_\odot$
R_*	Stellar radius	$2.5\ R_\odot$
T_*	Stellar effective temperature	4000 K
Σ	Disk surface density	$10^3 a_{\mathrm{AU}}^{-3/2}$ g cm^{-2}
a_i	Inner disk radius	$6\ R_* = 0.07$ AU
a_o	Outer disk radius	$23000\ R_* = 270$ AU
κ_V	Dust opacity at visual wavelengths[a]	400 cm^2 g^{-1}
ε_ν	Grain emissivity	$\begin{cases} 1 & \text{if } \lambda \le 2\pi r, \\ \left(\dfrac{2\pi r}{\lambda}\right)^\beta & \text{otherwise} \end{cases}$
r	Grain radius	0.1 μm
β	Grain emissivity index	1

[a] Absorption by dust grains is assumed to dominate the continuum opacity from visible through millimeter wavelengths.

and the gas density in the interior

$$\rho_{\mathrm{gi}} = \frac{1}{\sqrt{2\pi}} \frac{\Sigma}{h} \exp\left(-\frac{z^2}{2h^2}\right). \qquad (2)$$

Both the gas scale height, h, and interior temperature, T_i, take on different forms depending on the vertical optical depth of the interior. Inside 84 AU, the interior is opaque to its own reprocessed radiation, and

$$T_i \approx \frac{150}{a_{\mathrm{AU}}^{3/7}}\ \mathrm{K}\ , \qquad (3a)$$

$$h/a \approx 0.04 a_{\mathrm{AU}}^{2/7}\ . \qquad (3b)$$

Between 84 and 209 AU, the interior is optically thin to its own radiation but still thick to radiation from the surface; here

$$T_i \approx 21\ \mathrm{K}\ , \qquad (3c)$$

$$\frac{h}{a} \approx 0.15\left(\frac{a_{\mathrm{AU}}}{84}\right)^{1/2}\ . \qquad (3d)$$

Finally, in the outermost regions of the disk, the encased material is transparent to radiation from the surface, and

$$T_i \approx 21\left(\frac{209}{a_{\mathrm{AU}}}\right)^{19/45}\ \mathrm{K}\ , \qquad (3e)$$

$$\frac{h}{a} \approx 0.23\left(\frac{a_{\mathrm{AU}}}{209}\right)^{13/45}\ . \qquad (3f)$$

Boundary conditions are as follows. The superheated layer is located at $|z| = H \approx 4h$. Its visual optical depth normal to its flared surface is equal to the angle α at which stellar rays penetrate the disk (see Fig. 3 of CG97):

$$\alpha \approx \frac{0.4\ R_*}{a} + a\,\frac{d}{da}\left(\frac{H}{a}\right). $$

Radially, the disk extends from the silicate condensation boundary at a_i, to an outer radius, a_o, at which $H \approx a$.

The occulting angle,

$$\theta_0 \equiv \arctan\frac{a_o}{H(a_o)} = 45°\ , $$

is a natural angle with which to compare the viewing angle θ. For $\theta \lesssim \theta_0$, both the central star and most of the disk surface are in direct view. For $\theta \gtrsim \theta_0$, star and inner disk are blocked from view by the flared outer "wall."

2.2. Interior SED versus Θ

For clarity, we first consider only the disk interior. Figure 1 depicts the viewing geometry and coordinate system. Define x and y to be orthogonal spatial axes in the plane of the sky, centered on the star. The SED is the integral of specific intensity over projected disk area, viz.,

$$L_\nu \equiv 4\pi d^2 \nu F_\nu = 8\pi\nu \int_0^{a_o} dx \int_{-y(x)}^{y(x)} dy I_\nu\ , $$

where

$$y(x) = \sqrt{a_o^2 - x^2}\,\cos\theta + H(a_o)\sin\theta $$

traces the disk boundary on the sky, d measures distance to the source from Earth, and $I_\nu(x, y)$ is the specific intensity;

$$I_\nu = I_{\nu,i} = \kappa_V\,\varepsilon_\nu \int_0^\infty dl\rho_{\mathrm{gi}}\,B_\nu(T_i)\exp\left(-\tau_\nu\right)\ , $$

with

$$\tau_\nu = \kappa_V\,\varepsilon_\nu \int_0^l d\tilde{l}\rho_{\mathrm{gi}}\ . $$

Here B_ν is the Planck function, and l and $\tilde{l}$ both measure line-of-sight distance from the observer. Since temperature, density, and opacity are specified by our model, calculating the SED at arbitrary inclination is primarily an exercise in multidimensional integration. We perform these integrals numerically using standard techniques (Press et al. 1992). Optical depths are evaluated using a Romberg integrator with a mandated fractional accuracy of 10^{-3}. Specific intensities are computed on an adaptive step size grid, where the source function (B_ν) changes by no more than 20% between adjacent grid points. Integrals over y are performed using either a Romberg integrator or, in cases where the integrand is very sharply peaked and the Romberg integrator takes prohibitively many steps, a 60-point Gaussian quadrature routine. The final integration over x employs the trapezoidal rule on a 60-point logarithmic grid. Answers are routinely checked for robustness against changes in step size. We verify that the SED for $\theta = 0°$ computed using the multidimensional integration code matches the SED for
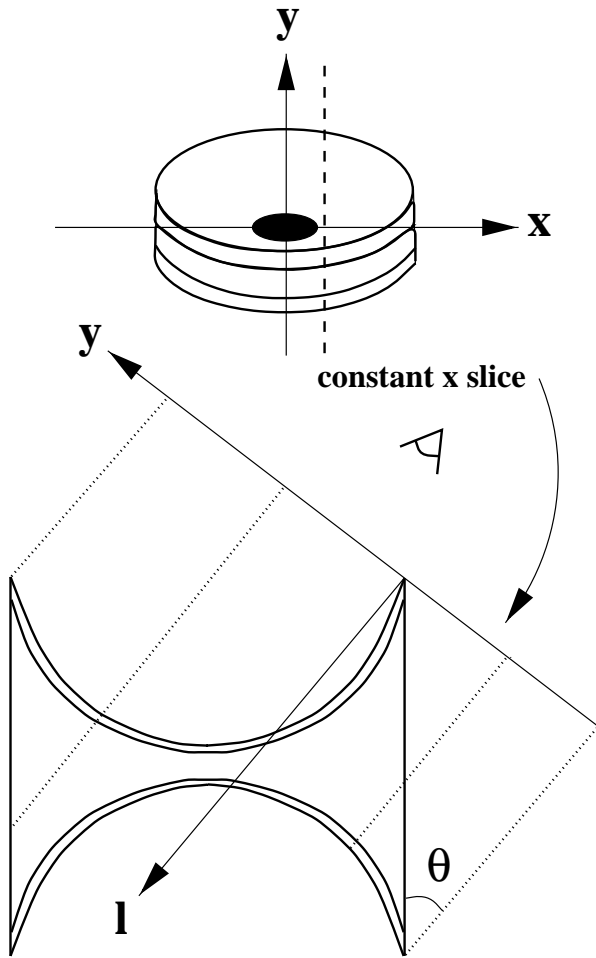
FIG. 1.—Schematic of viewing geometry and coordinate system. The disk interior is capped above and below by the superheated surface. To calculate the SED, specific intensities along lines of sight (dotted lines parallel to l) are summed over the projected disk area in x and y. Here θ is slightly less than the occulting angle θ_0.

face-on disks computed using the one-dimensional integrator of CG97.

Figure 2 displays a family of interior SEDs for different θ. First consider SEDs for angles $\theta \leq \theta_0(\theta = 0°, 30°, 45°)$.
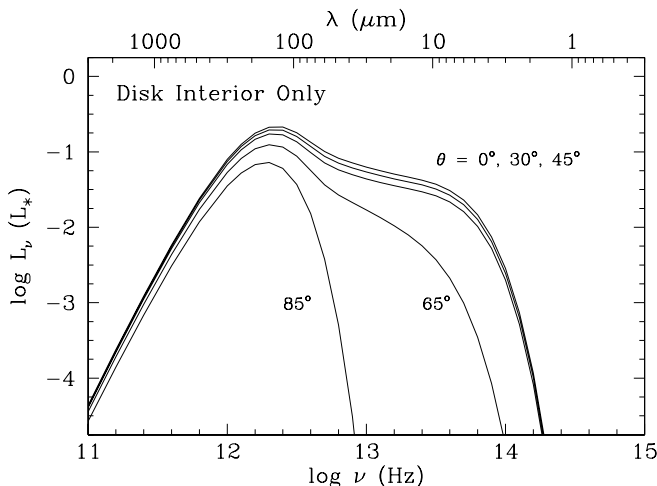

FIG. 2.—SED of the disk interior only, as a function of viewing angle. Short-wavelength emission from the inner disk is extinguished by the intervening outer disk for $\theta > \theta_0$. L_* denotes the luminosity of the central star.
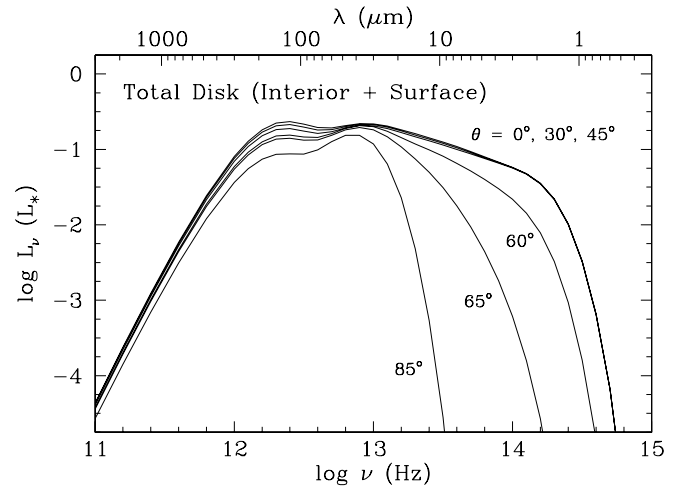

FIG. 3.—SED of the entire disk (interior plus surface) as a function of viewing angle. For $\theta < \theta_0$, the SED is insensitive to viewing aspect since short-wavelength radiation originates from the optically thin surface, while long-wavelength radiation is emitted by the optically thin interior. For $\theta > \theta_0$, the intervening outer disk dramatically extinguishes surface radiation at the shortest wavelengths.

Radiation at wavelengths shorter than ~ 100 μm comes mainly from optically thick regions; consequently, L_ν is approximately proportional to the areal projection factor $\cos \theta$. At longer wavelengths, the radiation is emitted by increasingly transparent material, so that L_ν tends to be independent of orientation.

For angles $\theta > \theta_0(\theta = 65°, 85°)$, short-wavelength emission from the inner disk is strongly extincted by the intervening outer disk. However, millimeter-wavelength fluxes drop by only a factor of 1.8 as the disk is viewed increasingly edge-on, since about half of the outer disk remains visible in that limit.

2.3. Superthermal plus Interior SED versus Θ

Next we compute the total SED. The superheated layer is treated as a plane-parallel atmosphere having visual optical depth α normal to the surface. Whenever a line of sight intersects the surface, we increment the specific intensity from the interior by[3]

$$\Delta I_\nu = B_\nu(T_{\rm ds})\left[1 - \exp\left(-\frac{\alpha \varepsilon_s}{|\hat{n} \cdot \hat{l}|}\right)\right] \exp\left(-\tau_{\nu,l}\right).$$

Here, $\hat{n}$ and $\hat{l}$ are unit vectors normal to the surface and parallel to the line of sight, respectively, ε_s is the Planck-averaged dust emissivity at the surface, and $\tau_{\nu,l}$ is the intervening optical depth between disk surface and observer.

Figure 3 displays a family of total disk SEDs labeled by θ. The behavior of the SED for $\lambda \gtrsim 80$ μm is similar to that described in § 2.2, since the interior dominates emission at those wavelengths.

Shortward of ~ 80 μm, emission from the superheated surface makes a qualitative difference to the appearance of

---

[3] This prescription fails for lines of sight which graze the surface tangentially. However, their fractional contribution to the integrated flux is of order $(h_s/R)^{1/2}$, where $h_s \approx (\partial \ln \rho_{\rm gi}/\partial z)^{-1}|_{z=H}$ is the geometrical thickness of the surface, and R is the radius of curvature of H. Since this fraction is less than 10%, for computational simplicity we let the intersected optical depth of the surface be $\alpha \varepsilon_s \times \min(|\hat{n} \cdot \hat{l}|^{-1}, 20)$.
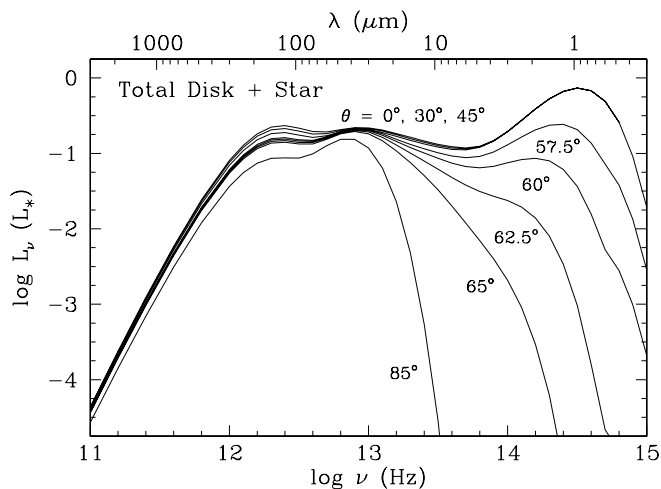
FIG. 4.—SED of the entire disk plus central star, as a function of viewing angle. At $\theta = 60°$, the visual optical depth to the star is $\tau_{*,V} = 4.5$. At $\theta = 65°$, $\tau_{*,V} = 22$. At $\theta = 85°$, $\tau_{*,V} = 7.6 \times 10^5$.

the SEDs. One difference is that for angles $\theta \leq \theta_0$, the flux is remarkably insensitive to viewing geometry.[4] This is because shorter wavelength radiation emerges primarily from the superheated surface layers, which are optically thin along most lines of sight.

For angles $\theta > \theta_0$, the intervening outer disk dramatically extinguishes surface radiation at the shortest wavelengths. However, the total disk SED between 30 and 80 μm is relatively robust to changes in inclination; it decreases by less than a factor of 3 between face-on and edge-on orientations. Radiation at these wavelengths originates from surface layers at large radii and is only slightly obscured by the tenuous interior at still larger radii.

Finally, in Figure 4 we add the contribution from the central star to the SED. The stellar flux fades rapidly with increasing θ beyond $\sim 55°$.

3. SPECTRAL DUST FEATURES

When viewed nearly face-on, passive disks exhibit emission lines associated with dust grain resonances. These features arise from material along the line of sight, which is optically thin: line-to-continuum flux ratios are of the same order as the percentage enhancement in line opacity. Emission lines may originate from both the optically thin superheated surface (as discussed in CG97) and the optically thin interior.

How do such lines vary as the disk is viewed increasingly edge-on? Might they appear in absorption instead, as Cohen & Witteborn (1985) find for seven of the 32 T Tauri stars they survey spectrophotometrically? To address these questions, we add six Gaussian-shaped spectral resonances to our grain emissivity law. In choosing resonant wavelengths and strengths, we aim to illustrate the range of effects that occur with variable viewing angle. Roughly, our six lines can be associated with crystalline H_2O ice at 60 and 100 μm (Waters & Waelkens 1998), amorphous silicates

---

[4] Slight reductions in midinfrared flux still occur for $\theta \leq \theta_0$, both because surface layers intermediate in radius are seen through the outer disk's atmosphere and because emission from the optically thick interior is proportional to the projected area.

---

at 10 and 20 μm (Mathis 1990), and small carbon-rich grains or polycyclic aromatic hydrocarbons (PAHs) at 3.3 and 6.2 μm (Waelkens et al. 1996).

Solid-state line spectra at various disk inclinations are displayed in Figure 5. Emission at all wavelengths varies little with viewing geometry for angles $\theta \lesssim \theta_0$. This is true particularly at the shortest wavelengths where lines arise largely from the optically thin surface layers. At wavelengths progressively longer than ~ 30 μm, the optically thin interior at large radius contributes increasingly to line emission. The drop in the long-wavelength continuum with increasing inclination reflects the $\cos \theta$ dependence of radiation emitted by the optically thick interior.

Emission lines at ~ 60 and 100 μm persist at angles $\theta \gtrsim \theta_0$, although their fluxes are lower by a factor of ~ 2 for edge-on as compared to face-on disks. For edge-on orientations, only about half of the optically thin interior remains visible. Emission around 20 μm is more robust to changes in inclination; most of this radiation emerges from the superheated surface at large radii and passes through the rarefied disk interior at yet larger radii with little attenuation.

At the shortest wavelengths, where occultation of the inner disk is significant, lines indeed appear in absorption, although only over a limited range of inclinations between θ_0 and 90°. For a dust grain resonance to appear in absorption, disk inclinations must be sufficiently high that line emission from the superheated surface is extinguished. However, θ cannot be so high that line and continuum optical depths both exceed unity at large radius where the disk interior is nearly isothermal. Only over an intermediate range of inclinations does radiation on and off the resonant wavelength probe a variety of interior disk temperatures. For the 3.3 μm resonance to appear in absorption, $60° \lesssim i \lesssim 65°$. At 6.2 μm, opacities are lower, and inclinations needed for absorption higher: $65° \lesssim i \lesssim 70°$. In principle, near-infrared line spectra may provide a sensitive diagnostic of disk inclination.

While the trends outlined above apply qualitatively to all passive disks, quantitative conclusions are model dependent. For example, in our standard model, no absorption line at 10 μm appears because line-of-sight optical depths
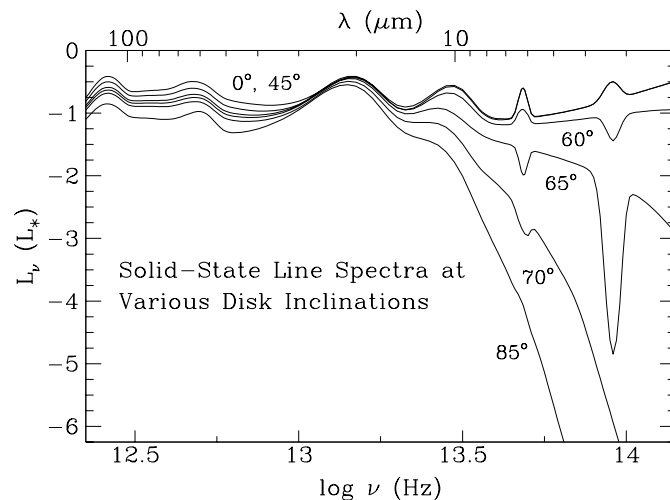

FIG. 5.—Solid-state line spectra at various disk inclinations. Resonances at the shortest wavelengths where opacities are highest appear in absorption over a limited range of viewing angles between θ_0 and 90°. Longer wavelength features persist in emission.

are too small to extinguish emission from the superthermal surface. However, such an absorption line would appear in the SED of a sufficiently massive, inclined disk.

4. APPLICATIONS TO OBSERVATIONS

4.1. *GM Aurigae and Central Holes*

GM Aur is a particularly clean, well-studied T Tauri system to which we can apply our SED models. The single central star has a mass of 0.72 $M_\odot$, luminosity of 0.7 $L_\odot$, and an age of 2×10^6 yr (Beckwith et al. 1990). Aperture synthesis maps in ^{13}CO$(2 \rightarrow 1)$ evince a rotating circumstellar gas disk having approximate projected dimensions 950×530 AU, inclined at $\theta \approx 30^\circ$ (Koerner, Sargent, & Beckwith 1993). *Hubble Space Telescope* (*HST*) images in scattered visible light reveal the disk surface to be flared and suggest i is closer to $\sim 60^\circ$ (Koerner 1997; Stapelfeldt et al. 1997). These same observations detect no outflow or remnant envelope surrounding this relatively evolved system.

CG97 model the SED of GM Aur, but with a face-on disk. They suggest that a nonzero disk inclination might cause line-of-sight radiation from the inner disk to be absorbed by the outer disk, thereby explaining the relatively low 12 μm flux without invoking a central hole. Here we investigate this possibility by refitting the SED with an inclined disk.

Figure 6 displays our new fit with a disk inclined at $\theta = 59^\circ$. Despite the nonzero inclination, none of our fit parameters changes significantly from those given by CG97 for the face-on case. Fluxes at *IRAS* wavelengths emerge mainly from the optically thin surface layers, and those at millimeter wavelengths emerge mostly from the optically thin interior; neither is sensitive to viewing angles θ near or less than θ_0.[5] Therefore, our fitted inclination does not reflect the shape of the IR SED; rather, it is chosen to reproduce the observed modest visual extinction to the central star of $A_V = 0.5$ mag and to conform with the imaging data.
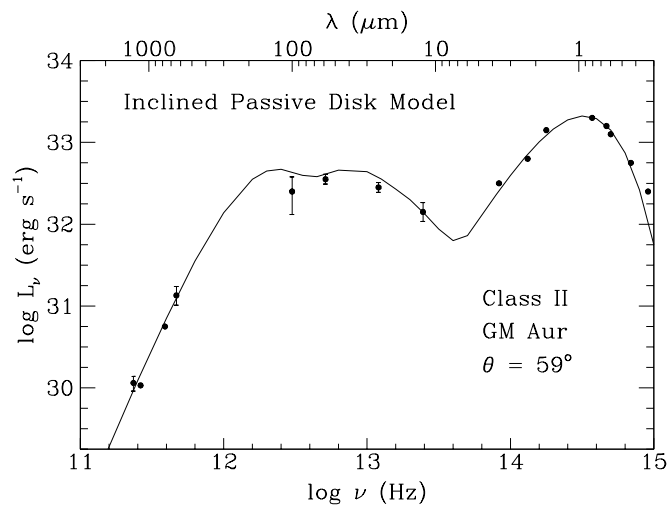
Matching the visual extinction comes at the cost of still requiring a large central gap having a radius ~ 60 times greater than the dust sublimation radius: $a_i = 4.8 \pm 2.7$ AU, where the uncertainty reflects that of the 12 μm *IRAS* point. There is no inclination for which the outer edge of our model disk attenuates the 12 μm flux without also extinguishing central starlight by several magnitudes. Line-of-sight column densities to surface regions inside ~ 5 AU (where most of the 12 μm emission originates) are only $\sim 20\%$ greater than the column density to the star. This small difference in the amount of obscuring material is completely insignificant; the opacity at 12 μm is 13 times lower than at visible wavelengths. Thus the low visual extinction to the central star implies that we should have a clear view of disk regions inside a few AU at near-infrared wavelengths.

In spite of these considerations, we remain skeptical of the existence of such a large central gap devoid of dust. A more palatable alternative might be that the inner disk's aspect ratio does not increase monotonically with radius. Such undulations in the height of the surface would shadow annular regions from the central star and lower their temperatures. In addition, those ripples nearest the observer would hide their warmer, starlit sides when viewed at nonzero inclination. Accretional heating may be responsible for such changes in surface geometry, as mentioned in CG97 (see their § 3.5); as estimated there, enhancements in disk thickness due to heating of the midplane may become significant inside a few AU. For an accretion disk that derives its luminosity solely from local viscous dissipation, the aspect ratio indeed decreases with radius whenever opacities increase steeply with temperature, as demonstrated by Bell et al. (1997).

4.2. *Class I Sources as Inclined Class II Sources*

Might some class I spectra represent T Tauri stars obscured by inclined disks? The possibility should be entertained for sources such as $04108+2803$B; Figure 7 demonstrates that a passive disk inclined at 65° provides a
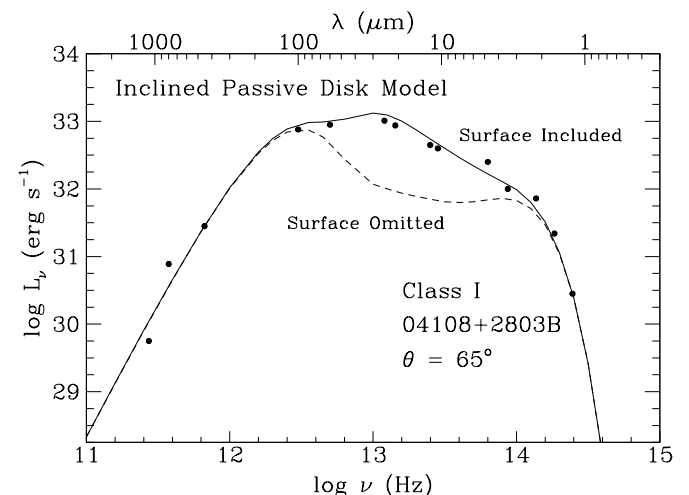

FIG. 6.—Observed SED (*filled circles*) of GM Aur and accompanying inclined passive disk model. Fit parameters are as follows: $\theta = 59^\circ$, $\Sigma = 2 \times 10^3 a_{\mathrm{AU}}^{-3/2}$ g cm^{-2}, $\beta = 1.4$, $r = 0.3$ μm, $a_o = 311$ AU (which implies $\theta_0 = 51^\circ$), and $a_i = 4.8$ AU. The formal requirement of a large AU-sized central gap persists despite accounting for a nonzero viewing angle.

[5] θ_0 for this disk equals 51°.

FIG. 7.—Observed SED (*filled circles*) of class I source $04108+2803$B (Kenyon et al. 1993a) and accompanying inclined passive disk model. Fit parameters for the disk are as follows: $\theta = 65^\circ$, $\Sigma = 0.3 \times 10^3 a_{\mathrm{AU}}^{-3/2}$ g cm^{-2}, $\beta = 1.2$, $r = 0.1$ μm, $a_o = 270$ AU (which implies $\theta_0 = 46^\circ$), and $a_i = 0.07$ AU. Stellar parameters are identical to those of our standard model T Tauri star.

reasonable fit (to within factors of 2) to this class I SED. Fit parameters are similar to those of our standard model and are listed in the figure caption. For this particular model, near-IR emission at J, H, and K is interpreted as central starlight extincted by the disk's outer edge; inclusion of starlight scattered off the disk surface would imply a larger inclination. To highlight the contribution from the superheated surface, we also plot the SED with the surface emission removed. Fluxes between 3 and 60 μm arise primarily from the superthermal surface, seen both through and over the lip of the outer disk atmosphere (see Fig. 1).

Clearly, a class I SED does not imply a unique distribution of circumstellar material. High angular resolution images provide additional clues. Many class I sources exhibit near-IR nebulosity on scales ranging from 1500 to 3000 AU (Kenyon et al. 1993b, and references therein); for these sources, an additional, nondisk component of dust is needed. Kenyon, Calvet, & Hartmann (1993a) model class I SEDs using rotationally flattened, infalling envelopes that are passively heated by central stars. These envelopes extend out to larger radii than do our disks, typically 3000 AU, but contain roughly the same amount of mass, about 0.1 $M_\odot$. Bipolar holes empty of material, presumably evacuated by outflows, are invoked so that central starlight may scatter off cavity walls toward Earth, thereby explaining the observed near-IR fluxes. In imaging observations of three class I sources using the Near Infrared Camera and Multi-Object Spectrometer (NICMOS) of *HST*, Padgett et al. (1999) discover nearly edge-on, flared circumstellar disks having diameters 300–750 AU. Near-IR emission is observed to be scattered not only off upper and lower disk surfaces, but also off "dusty material within or on the walls of outflow cavities."

In general, a combination of an inclined, passively heated disk and a dusty bipolar outflow or partially evacuated envelope may best describe class I sources. Since 04108 + 2803B reveals no optical or near-IR emission beyond $\sim$140 AU from its central star (Kenyon et al. 1993a), it is consistent with being a limiting example of a simple inclined disk. Two other examples for which this limiting case scenario may also apply include the embedded sources 04295 + 2251 and 04489 + 3042. Both sources exhibit nearly flat excesses between $\sim$3 and 100 μm, which may arise from flared circumstellar disks. Neither source betrays extended near-IR emission on scales greater than a few hundred AU, or high-velocity molecular gas from an outflow (Kenyon et al. 1993b).

Near-IR polarimetry also addresses the possible presence of envelopes. Whitney, Kenyon, & Gómez (1997) determine that linear polarizations greater than $\sim$20% at J, H, and K characterize the largest reflection nebulae associated with class I sources. Such large polarizations are interpreted as arising from the scattering of central starlight off cavity walls in envelopes. In contrast, 04108 + 2803B evinces fractional polarizations of 5.1% and 1.6% at H and K, respectively (Whitney et al. 1997)—levels more comparable to those in class II sources than in truly younger, more embedded protostars, and which may arise from starlight scattered off the disk surface. Resolved polarimetry maps of 04108 + 2803B can test our hypothesis.

Degeneracies inherent in models deduced from an SED may also be broken by kinematic studies. Interferometric radial velocity maps in molecular lines may distinguish between an infalling envelope (see, e.g., Hayashi, Ohashi, & Miyama 1993; Ohashi et al. 1997) and a rotating disk (see, e.g., Koerner & Sargent 1995).

Terquem & Bertout (1996) also independently model 04108 + 2803B as a T Tauri star embedded within a dynamically warped disk. The antisymmetric warp considered by these authors is tidally induced by a hypothetical stellar companion in an orbit inclined to the primary's disk. High spatial resolution images (e.g., from speckle interferometry) can test for possible multiplicity and telltale signs in disk geometry.

Finally, we note that the inverse problem to 04108 + 2803B is presented by the star HK Tau B: a system observed to possess an edge-on ($i \approx 85°$) circumstellar disk of the kind described in this paper and no observable envelope, but whose IR SED is not well measured because of confusion from an IR-bright companion (Stapelfeldt et al. 1998; Koresko 1998). We await the *Space Infrared Telescope Facility* (*SIRTF*), which can provide both the SED between 3 and 180 μm and images of the superheated disk surface in thermal emission.

REFERENCES

Beckwith, S. V. W., Sargent, A. I., Chini, R. S., & Gusten, R. 1990, AJ, 99, 924
Bell, K. R., Cassen, P. M., Klahr, H. H., & Henning, Th. 1997, ApJ, 486, 372
Calvet, N., Patiño, A., Magris, G., & D'Alessio, P. 1991, ApJ, 380, 617
Chiang, E. I., & Goldreich, P. 1997, ApJ, 490, 368 (CG97)
Cohen, M., & Witteborn, F. C. 1985, ApJ, 294, 345
D'Alessio, P., Cantó, J., Calvet, N., & Lizano, S. 1998, ApJ, 500, 411
Hayashi, M., Ohashi, N., & Miyama, S. M. 1993, ApJ, 418, L71
Kenyon, S. J., Calvet, N., & Hartmann, L. 1993a, ApJ, 414, 676
Kenyon, S. J., & Hartmann, L. 1987, ApJ, 323, 714
Kenyon, S. J., Whitney, B. A., Gomez, M., & Hartmann, L. 1993b, ApJ, 414, 773
Koerner, D. W. 1997, Origins of Life and Evolution of Biosphere, 27, 157
Koerner, D. W., & Sargent, A. I. 1995, Ap&SS, 223, 169
Koerner, D. W., Sargent, A. I., & Beckwith, S. V. W. 1993, Icarus, 106, 2
Koresko, C. D. 1998, ApJ, 507, L145
Lada, C. J. 1987, in IAU Symp. 115, Star Forming Regions, ed. M. Peimbert & J. Jugaku (Dordrecht: Reidel), 1
Lada, C. J., & Wilking, B. A. 1984, ApJ, 287, 610

Malbet, F., & Bertout, C. 1991, ApJ, 383, 814
Mathis, J. M. 1990, ARA&A, 28, 37
Mendoza, E. E. V. 1968, ApJ, 151, 977
Ohashi, N., Hayashi, M., Ho, P. T. P., & Momose, M. 1997, ApJ, 475, 211
Padgett, D. L., Brandner, W., Stapelfeldt, K. R., Strom, S. E., Terebey, S., & Koerner, D. 1999, AJ, in press
Press, W. H., Teukolsky, S. A., Vetterling, W. T., & Flannery, B. P. 1992, Numerical Recipes in Fortran (Cambridge: Cambridge Univ. Press)
Shu, F. H., Adams, F. C., & Lizano, S. 1987, ARA&A, 25, 23
Stapelfeldt, K., Burrows, C. J., Koerner, D., Krist, J., Watson, A. M., Trauger, J. T., & WFPC2 Image Development Team. 1997, in ESO Symp., Science with the VLT Interferometer, ed. F. Paresce (Berlin: Springer), 395
Stapelfeldt, K. R., Krist, J. E., Ménard, F., Bouvier, J., Padgett, D. L., & Burrows, C. J. 1998, ApJ, 502, L65
Terquem, C., & Bertout, C. 1996, MNRAS, 279, 415
Waelkens, C., et al. 1996, A&A, 315L, 245
Waters, L. B. F. M., & Waelkens, C. 1998, ARA&A, 36, 233
Whitney, B. A., Kenyon, S. J., & Gómez, M. 1997, ApJ, 485, 703